Structure
Article

PagP Crystallized from SDS/Cosolvent Reveals the Route for Phospholipid Access to the Hydrocarbon Ruler

Jose Antonio Cuesta-Seijo,[1] Chris Neale,[2,3] M. Adil Khan,[4] Joel Moktar,[4] Christopher D. Tran,[1] Russell E. Bishop,[4] Régis Pomès,[2,3] and Gilbert G. Privé[1,3,5,*]
[1]Division of Cancer Genomics and Proteomics, Ontario Cancer Institute and Campbell Family Cancer Research Institute, 101 College Street, Toronto, ON M5G 1L7, Canada
[2]Molecular Structure and Function, The Hospital for Sick Children, 555 University Avenue, Toronto, ON M5G 1X8, Canada
[3]Department of Biochemistry, University of Toronto, Toronto, ON M5S 1A8, Canada
[4]Department of Biochemistry and Biomedical Sciences, and the Michael G. DeGroote Institute for Infectious Disease Research, McMaster University, Hamilton, ON L8N 3Z5, Canada
[5]Department of Medical Biophysics, University of Toronto, Toronto, ON M5G 2M9, Canada
*Correspondence: prive@uhnres.utoronto.ca
DOI 10.1016/j.str.2010.06.014

SUMMARY

Enzymatic reactions involving bilayer lipids occur in an environment with strict physical and topological constraints. The integral membrane enzyme PagP transfers a palmitoyl group from a phospholipid to lipid A in order to assist *Escherichia coli* in evading host immune defenses during infection. PagP measures the palmitoyl group with an internal hydrocarbon ruler that is formed in the interior of the eight-stranded antiparallel β barrel. The access and egress of the palmitoyl group is thought to take a lateral route from the bilayer phase to the barrel interior. Molecular dynamics, mutagenesis, and a 1.4 Å crystal structure of PagP in an SDS / 2-methyl-2, 4-pentanediol (MPD) cosolvent system reveal that phospholipid access occurs at the crenel present between strands F and G of PagP. In this way, the phospholipid head group can remain exposed to the cell exterior while the lipid acyl chain remains in a predominantly hydrophobic environment as it translocates to the protein interior.

INTRODUCTION

PagP is an integral membrane enzyme that transfers a palmitoyl group from the *sn*-1 position of a glycerophospholipid to the lipid A (endotoxin) moiety of lipopolysaccharide (LPS) resulting in the production of a palmitoylated lipid A and a lysophospholipid by-product. The donor phospholipid, LPS acceptor, and enzyme active site are all located in the external-facing leaflet of the Gram-negative outer membrane (Figure 1) (Bishop et al., 2000; Jia et al., 2004; Khan and Bishop, 2009; Smith et al., 2008). The enzyme provides bacterial resistance to host immune defenses involving cationic antimicrobial peptides (Guo et al., 1998), attenuates the host inflammatory response to infection triggered by the TLR4/MD2 pathway (Kawasaki et al., 2004; Muroi et al., 2002; Tanamoto and Azumi, 2000), and is a virulence determinant to infection by certain pathogens (Piliione et al., 2004; Preston et al., 2003; Robey et al., 2001). The protein belongs to the PhoP/PhoQ-regulon, which controls the expression of bacterial genes needed for covalent lipid A modifications induced during infection by antimicrobial peptides (Bader et al., 2005). PagP is a potential target for the development of anti-infective agents and a tool for the synthesis of lipid A-based vaccine adjuvants and endotoxin antagonists (Bishop, 2005; Raetz et al., 2007).

As an enzyme of lipid metabolism, PagP is remarkable in its ability to select a 16-carbon saturated palmitate chain to the exclusion of all other acyl chain types present within the membrane pool of glycerophospholipids (Bishop et al., 2000). The enzyme is an eight-stranded β barrel (Hwang et al., 2002) whose catalytic mechanism likely involves cycling between two dynamically distinct states (Hwang et al., 2004), although the details of the reaction remain unknown. The crystal structure of PagP determined in the presence of the nondenaturing detergent lauryldimethylamine oxide (LDAO) (Ahn et al., 2004) revealed a detergent molecule bound in the interior of the barrel with the head group pointing toward the extracellular side of PagP. This detergent molecule marks the position of the hydrocarbon ruler, which selects acyl chains in the glycerophospholipid substrate with methylene unit resolution (Ahn et al., 2004; Khan et al., 2007, 2010). A recent simulation study of PagP has examined the solvation, but not the binding, of the enzyme by detergent and lipid molecules (Cox and Sansom, 2009).

We have recently reported that certain water miscible amphipathic alcohols, notably 2-methyl-2,4-pentanediol (MPD) can modulate the protein-binding properties of SDS so that the detergent behaves essentially as a ''gentle'' nondenaturing detergent (Michaux et al., 2008a; Privé, 2007). Under typical conditions, SDS is a strongly denaturing anionic detergent that is widely used in biochemical applications to solubilize proteins in a denatured state (Helenius and Simons, 1975). It is effective at millimolar concentrations and induces a nonnative structure with a high proportion of α helix, although its mechanism of action is not well understood (Guo et al., 1990; Manning and Colon, 2004; Mattice et al., 1976; Nielsen et al., 2007; Otzen,

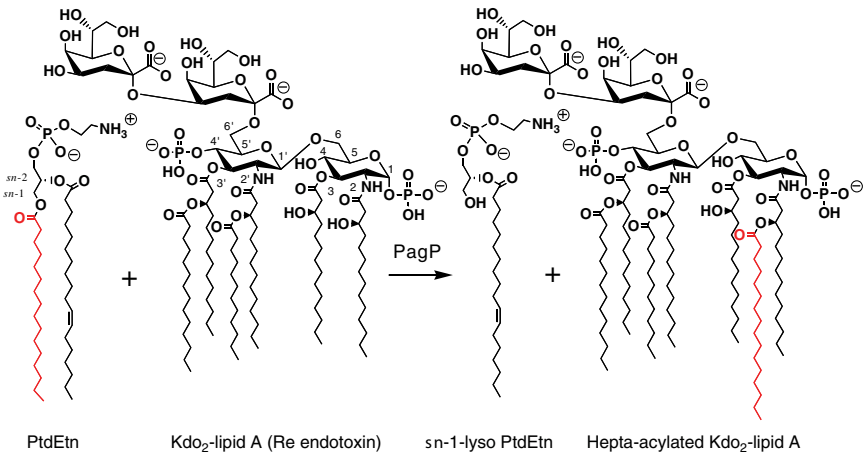

Figure 1. Reaction Catalyzed by PagP

PagP catalyzes the transfer of a palmitate chain (shown in red) from the *sn*-1 position of phosphatidylethanolamine (PtdEtn) to lipopolysaccharide (LPS), shown here as Kdo_2-lipid A (Re endotoxin). This lipid consists of lipid A linked at the 6′ position with two units of 3-deoxy-D-*manno*-2-octulosonic acid (Kdo). Lipid A is a β-1′,6-linked disaccharide of glucosamine that is acylated with *R*-3-hydroxymyristate chains at the 2, 3, 2′, and 3′ positions, and phosphorylated at the 1 and 4′ positions. Acyloxyacyl linkages with laurate and myristate chains at the 2′ and 3′ positions, respectively, provide the constitutive hexa-acylated lipid A, which is a potent endotoxin. A regulated proportion of lipid A in *E. coli* contains a palmitate chain (16:0) in acyloxyacyl linkage at position 2 (in red in the figure), which yields a hepta-acylated molecule with attenuated endotoxic properties.

2002; Otzen and Oliveberg, 2002; Reynolds and Tanford, 1970; Samso et al., 1995; Smith, 1994). MPD is best known as a protein precipitant in crystallization experiments (Anand et al., 2002). Concentrations of 1–2 M MPD protected both soluble and integral membrane proteins from SDS denaturation, and several proteins, including PagP, could be induced to fold from the SDS denatured state upon addition of MPD (Michaux et al., 2008a). PagP in SDS/MPD could be reversibly denatured and refolded upon heating and cooling cycles, confirming that the folded protein is at thermodynamic equilibrium in this detergent/cosolvent system.

Here, we report the 1.4 Å crystal structure of PagP crystallized directly from SDS/MPD. The barrel structure of PagP in SDS/MPD is similar to the previously determined crystal structure in LDAO (Ahn et al., 2004) and with the solution NMR structures in dodecylphosphocoline (DPC) and β-D-octyl-glucoside (OG) (Hwang et al., 2002). However, we observed differences in the conformations of the four extracellular loops, indicating regions of flexibility in the protein that may be important for substrate binding and catalysis. Like a parapet that surrounds the turret of a medieval castle, the PagP β barrel contains indentations known as the crenel and embrasure, which provide gateways for lateral lipid access between the membrane external leaflet and the hydrocarbon ruler. Cysteine crosslinking between these regions of diminished β strand hydrogen bonding has previously identified the crenel between strands F and G as the palmitoyl chain access route, whereas the embrasure at the β-bulge between strands A and B serves as the egress route for the chain following the coupling to lipid A acceptor (Khan and Bishop, 2009). We now use molecular dynamics simulations and mutagenesis to confirm a phospholipid access route via the F/G crenel coupled to a movement of extracellular loop L4. We identify Tyr147 in L4 as a potential gating residue controlling lateral access of phospholipids to the interior hydrocarbon ruler pocket of PagP.

RESULTS

Crystallization of PagP from SDS/MPD

E. coli PagP was directed to inclusion bodies by overexpressing the protein without a signal sequence (Ahn et al., 2004; Hwang et al., 2002). Washed inclusion bodies were dissolved in a buffer containing 1% SDS and 1 M MPD. The solution was heated to 100°C and the protein was refolded by slow cooling. Refolding was quantitative as judged by an SDS-PAGE assay (Michaux et al., 2008a). Circular dichroism confirmed that the refolded protein was predominantly β sheet and exhibited a characteristic exciton couplet at 232 nm indicating the correct formation of the hydrocarbon ruler (see Figure S1 available online) (Khan et al., 2007, 2010; Michaux et al., 2008a). No chromatographic steps were performed, and the only purification of the protein occurred during the initial preparation of the insoluble inclusion body material. The protein solution was concentrated to 5.8 mg/ml and contained 3.85% w/v SDS (135 mM) as measured by a methylene blue extraction assay (Arand et al., 1992). The critical micelle concentration (cmc) of SDS in 1 M MPD and 10 mM Tris-HCl is approximately 0.6 mM as measured by isothermal titration calorimetry (J. Holyoake and G.G.P., unpublished data), and so the SDS concentration in the final crystallization stock solution was over 250-fold above its cmc.

The protein was crystallized by the traditional hanging drop method by mixing equal volume solutions of the protein stock and a salt-rich reservoir containing 1 M MPD, and allowing vapor-phase equilibration between the protein droplet and the much larger volume of the reservoir solution. Two phases formed in the protein droplet as equilibration proceeded. Crystals nucleated at the interface of the two phases and grew exclusively into one of the phases. The fluorescent lipid NBD-DPPC (Avanti Polar Lipids) was added to a hanging drop containing crystals and the lipid dye partitioned preferentially into the phase in which the PagP crystals grew, suggesting that the SDS concentration in the phase that supported crystal growth was further enriched in detergent relative to the initial protein stock solution (Figure S2). Both the protein stock solution and the reservoir solution initially contained 1 M MPD, but because MPD is volatile, the MPD concentration in the phase containing the protein crystals is unknown. However, we located 10 MPD molecules in the final refined structure (see below), indicating a relatively high concentration of the cosolvent in the mother liquor surrounding the crystal.

Table 1. Data Collection and Refinement Statistics	
Data Collection	
Space group	$P6_222$
Unit cell (Å)	113.23, 113.23, 55.06
R_{sym} [a]	0.068 (0.531)
$I / \sigma(I)$	28.1 (1.3)
Completeness (%)	97.7 (80.4)
Redundancy	8.2 (4.1)
Refinement	
Resolution (Å)	20.0–1.40
No. reflections	40,392
R_{work} / R_{free}	0.171 (0.303)/0.208 (0.290)
Number of atoms	
Protein	1321
SDS	97 (6 molecules)
MPD	80 (10 molecules)
Ions	32
Water	56
B factors (Å^2)	
Protein	27.1
SDS	47.6
MPD	48.3
Ions	60.5
Water	38.1
Rmsd bond length (Å)	0.021
Rmsd bond angles (°)	2.12

[a] Values in parentheses are for the high-resolution shell from 1.42–1.40 Å.

Structure Overview

Full anisotropic refinement was performed to a resolution of 1.4 Å (Table 1). The structure is an eight-stranded β barrel that spans the membrane region with a leading amphipathic N-terminal α helix that lies at the interface between the periplasm and the outer membrane inner leaflet. The eight strands of the barrel are named A to H and the four extracellular loops are referred to as L1 to L4 (Figure 2). The hydrocarbon ruler pocket in the barrel interior is occupied by a SDS molecule in a position similar to the LDAO molecule found in the crystal structure determined in that detergent (Ahn et al., 2004).

The high resolution of this structure allowed us to trace all of the amino acids in the N-terminal α helix (Huysmans et al., 2007), which extends from Asn-1 to Trp-17. Loop L1 links strand A to strand B and is partly disordered, and amino acids 38–45 from this loop are not included in the final model. This loop was also not fully modeled in the LDAO crystal structure (Ahn et al., 2004) and is highly dynamic in the NMR structures (Hwang et al., 2002, 2004), indicating that this region is intrinsically disordered, at least in the absence of a lipid bilayer.

The overall barrel structure of PagP in SDS/MPD resembles that of PagP in LDAO by X-ray crystallography (Ahn et al., 2004) and in DPC or OG micelles by NMR (Hwang et al., 2002). Least-squares superposition of the Cα atoms from the β sheet residues in strands A–H of PagP results in an RMSD of 0.70 Å between the SDS/MPD and the LDAO structures (Figure 2A).

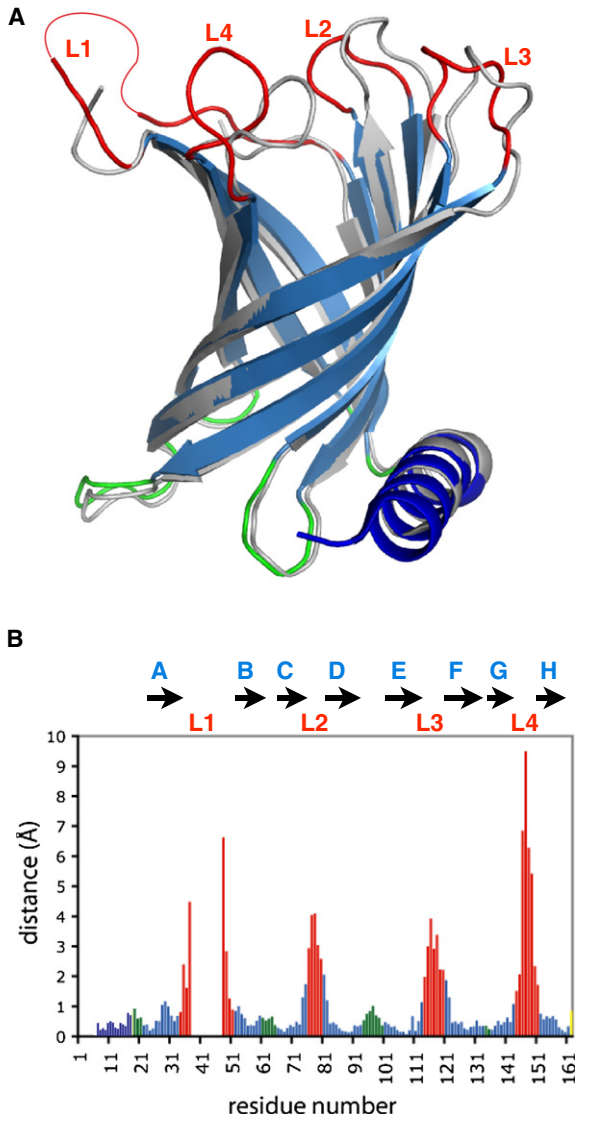

Figure 2. Differences between the SDS/MPD and the LDAO Crystal Structures of PagP

(A) Superposition of the SDS/MPD (blue, red, green) and LDAO (gray) crystal structures of PagP. The thin red line in L1 connects residue 37 to 46 and indicates the disordered region of this loop. Only the β sheet residues were used in the least-squares fitting.

(B) Distances between the α carbons of the SDS/MPD and the LDAO crystal structures of PagP. Residues in β strands are in blue, and only those were used for the superposition. The N-terminal helix is shown in dark blue, the periplasm-facing loops are in green, and the extracellular loops L1–L4 are in red. See also Figure S1.

The structures of the short periplasm-facing loops are also well conserved between the structures; however, deviations greater than 1.2 Å are seen in the four extracellular loop regions (Figure 2B). These extracellular loops are also the most dynamic regions of the protein as measured by NMR (Hwang et al., 2002, 2004).

Lattice forces may influence some of the loop conformations, as surfaces on both the periplasmic and extracellular sides of the

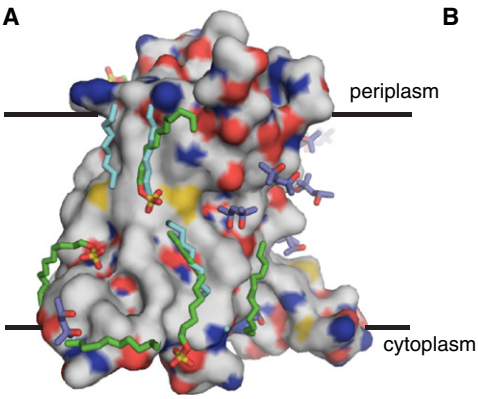

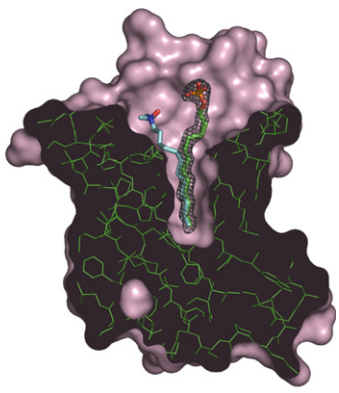

Figure 3. SDS and MPD Environment in the Crystal

(A) Externally associated SDS and MPD molecules are shown on the PagP solvent-accessible surface. PagP is colored with white carbons, red oxygens, blue nitrogens, and yellow sulfurs. The approximate position of the bilayer is indicated. The MPD molecules are shown with purple carbons and red oxygens. The SDS molecules are show with green aliphatic tails. The LDAO detergent coordinates from PDB ID 1THQ are included after superposition of the proteins and are shown with cyan carbons.

(B) The surface of PagP from the SDS/MPD structure is shown in pink, and a cut through the structure shows the pocket of the hydrocarbon ruler. The SDS molecule in the pocket is shown in stick representation with green carbons. The mesh shows the electron density for SDS in the 2Fo-Fc map contoured at 1.2σ. The LDAO molecule in the pocket of the LDAO crystal PDB ID 1THQ is shown with cyan carbons for comparison.

See also Movie S1 and Figure S2.

protein are involved in crystal packing contacts. This applies to both the SDS/MPD and LDAO structures, which adopt entirely different crystal lattices. The differences in the two structures are mostly in the extracellular loops, suggesting that these parts of the protein may be especially malleable. In fact, it is most likely the different lattice environments, rather than the influence of the SDS versus LDAO detergents per se, that have selected the different loop conformations. We suggest that the different crystal forms have selected two possible structural states for PagP. Such effects are common, and give insight into the flexibility of structures based on the static snapshots of single crystal structures. For example, a comparison of nine different structures of the HIV protease has been used to analyze the plasticity of the flap regions of the protein (Heaslet et al., 2007).

PagP/SDS Interactions

The final model contains six SDS molecules with an average B factor of 47 $Å^2$. In all cases the B factors are higher for the head group than for the aliphatic chain. Five of the SDS molecules are in contact with the exterior of the protein in the membrane-spanning region of PagP and are bound into crevices in the surface of the molecule (Figure 3A; Movie S1). The sulfate head groups do not make any consistent types of interactions with the protein and are consequently less ordered in the crystal. Thus, bound SDS molecules behave like other detergents in which binding to the protein is determined primarily by the aliphatic chain (Hunte and Richers, 2008; Qin et al., 2006). The structure of PagP crystallized from LDAO contains five ordered detergent molecules, four of which are common with the SDS binding sites (Figure 3A). The detergent molecules seen in the SDS/MPD structure are thus bound in general detergent binding sites that likely correspond to lipid acyl chain binding sites in the natural outer membrane environment of PagP. No significant SDS-SDS contacts are observed in the crystal and any micellar structures that may be present in the crystal are not ordered.

The remaining SDS molecule is found in the interior of PagP. The acyl chain binding pocket in the center of the β barrel is occupied by a detergent molecule in a similar fashion to that observed in LDAO (Ahn et al., 2004). This pocket is part of the hydrocarbon ruler of PagP that selects for palmitate chains in the *sn*-1 position of substrate phospholipids (Khan et al., 2007, 2010). The nine terminal carbons of the SDS molecule are found to be tightly held and have the lowest atomic B factors for this molecule. The B factors for carbons nearer to the head group increase significantly and the electron density becomes tubular in contrast to the zigzagging pattern of the lower part of the tail. The SDS in the pocket overlaps very well with the LDAO molecule in the terminal eight carbons in the acyl chain, but the paths diverge nearer to the head group region. As a result, the anionic SDS head group is located in a different position than the zwitterionic head group of LDAO (Figure 3B). The head group of SDS is closer to loop L1 and farther from L2, relative to the position of the LDAO head group.

PagP/MPD Interactions

The final model includes ten MPD molecules (Figure 3A; Movie S1). Seven of these are in conformations in which the two hydroxyl groups form intramolecular hydrogen bonds, such that the MPD molecules display a hydrophilic face and a hydrophobic face (Anand et al., 2002). Within the ordered molecules, there are no significant interactions between the MPD and SDS. A previous study also found no interactions between SDS and MPD in lysozyme crystals (Michaux et al., 2008b), and the present study expands this result to crystals of membrane proteins in which SDS is the stabilizing detergent.

Seven of the ten MPD molecules are bound to the hydrophobic membrane-exposed surface of PagP or to residues marking the transition between the hydrophobic and hydrophilic surfaces. These seven molecules are also in contact with hydrophilic residues of symmetry-related proteins and thus play important roles in building the crystal lattice. Overall, the MPD molecules are found in two types of environments in the crystal: they either fill in small deep pockets in the protein's surface or are sandwiched between relatively flat surfaces of two symmetry equivalent molecules. Four of the MPD molecules stack directly with π electronic clouds of the Trp17, Tyr23, Trp89, and Trp117 aromatic side chains of PagP. MPD has been used in the crystallization of at least 20 other integral membrane proteins based on data contained in the membrane protein data bank (http://www.mpdb.tcd.ie) (Raman et al., 2006). Ordered MPD molecules

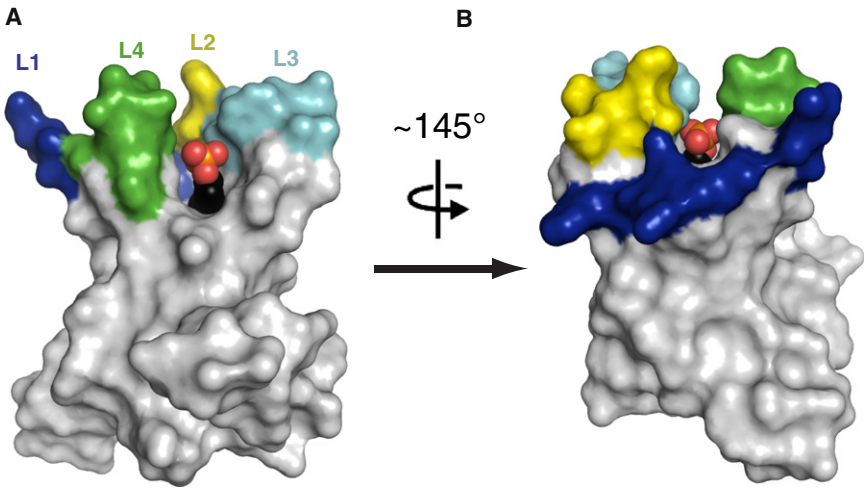

Figure 4. Crenels as Possible Routes in and out of the Hydrocarbon Ruler Pocket
PagP is shown in a surface representation with the β barrel and the periplasmic loops in white. Loop L1 is dark blue, L2 is yellow, L3 is cyan, and L4 is green. The SDS molecule buried within the hydrocarbon ruler pocket is shown as a space-filling model with black carbons, orange sulfur, and red oxygens. The SDS molecule is clearly visible through a crenel between strands F and G in (A) and through a crenel between strands B and C in (B). The F/G crenel is larger and deeper in the membrane than the B/C crenel.

have been reported in crystal structures of PagP in LDAO (Ahn et al., 2004), outer membrane phospholipase A (Snijder et al., 2001), OmpT (Vandeputte-Rutten et al., 2001), and BtuB crystallized from lipidic mesophase (Cherezov et al., 2006). In general, the MPD molecules in these structures occupy positions that are consistent with what we observe for PagP in SDS/MPD.

Catalytic Center

The conserved residues that are necessary for the catalytic activity of PagP include His33 in the extracellular loop L1 and Asp76 and Ser77 in L2 (Hwang et al., 2002). In the SDS/MPD structure, His33 is 13.0 Å away from Asp76 and 14.8 Å away from Ser77 (distances between α carbons; the distance between Oγ of Ser77 and Nε2 of His33 is 8.5 Å). These residues are closer than in the LDAO structure where the Cα distances are 16.4 and 17.0 Å respectively. This difference is mostly due to a rigid-body tilting of loop L2 toward L1, but the residues in the SDS/MPD structure are still too far apart to form a catalytic center. Thus, the formation of a competent active site likely involves additional rearrangements of the surface loops, possibly triggered by the binding of donor phospholipid and/or lipid A acceptor (Bishop, 2005; Raetz et al., 2007).

Accessibility of the Hydrocarbon Ruler Pocket

The SDS crystal structure shows that extracellular loop L4 moves away from the barrel interior, resulting in a large gap (a crenel) (Khan and Bishop, 2009) between strands F and G (Figure 4A). This gap opens a path to the top part of the hydrocarbon ruler that was blocked by the side chain of Tyr147 in the LDAO structure (Ahn et al., 2004). A smaller crenel is present between strands B and C (Figure 4B). As a result, we sought to further analyze possible access routes into and out of the barrel interior.

We analyzed the possible acyl chain entry and exit routes by performing nonequilibrium molecular dynamics simulations. We chose this approach in order to gain insight into the route(s) of acyl chain entry and exit that are most easily accommodated by the protein. This is an early step in the overall reaction, and the subsequent steps along the catalytic pathway likely involve larger scale motions of the protein backbone that are beyond the scope of these simulations. The strategy was to test a large number of short nonequilibrium simulations in order to generate an ensemble of trajectories, rather than to generate a smaller number of longer simulations that would provide limited statistical sampling. The 100 ps length of the simulations was sufficient to observe productive insertions and extractions, yet short enough to allow a large number of repeats for statistical significance. Overall, we generated 1205 insertion attempts and 302 extraction attempts.

PagP in the conformation from the SDS/MPD crystal was placed in an explicit phospholipid bilayer. No significant reorganization of the PagP backbone was observed during the simulations. Acyl-chain entry was assessed by applying a biasing force to the *sn*-1 chain of a 1-palmitoyl-2-oleoyl-*sn*-glycero-3-phosphocholine (POPC) molecule from the upper leaflet of the bilayer, directing it toward the empty PagP binding pocket. Of 1205 such simulations, 55 resulted in the *sn*-1 chain entering the binding pocket between strands F and G (the F/G route), five resulted in the *sn*-1 chain jumping out of the bilayer over the top of the protein near strands B to E, and in 1145 simulations the protein blocked the steered phospholipid from approaching the binding pocket more closely than other phospholipids in the first solvation shell (Figure 5A). Considering that the initial positions of the *sn*-1 acyl chain were distributed approximately uniformly around the barrel, roughly one-eighth of the 1205 binding simulations were directed at the F/G route. Thus, 55 of approximately 150 F/G attempts were successful, while none of the non-F/G route attempts were successful.

Next, acyl-chain exit was assessed by applying a biasing force to a dodecyl phosphate (DP) molecule placed in the binding pocket of PagP, compelling it to exit in the bilayer plane. Of 302 such simulations, 95 resulted in detergent extraction by the F/G route, 26 by the B/C route, and 181 extraction attempts ended with the detergent still inside the binding pocket (Figure 5B). The fact that the B/C route was identified as a viable route of acyl-chain extraction, but not insertion, is likely due in part to the tilt of PagP in the bilayer plane, which lowers the F and G strands into the hydrophobic region of the bilayer more than it lowers the B and C strands. This tilt is predicted by the hydrophobic surface potential and arrangement of aromatic belt residues (Ahn et al., 2004) and confirmed experimentally by measuring oxygen contacts by NMR (Evanics et al., 2006). Analogous simulations starting from the LDAO crystal structure

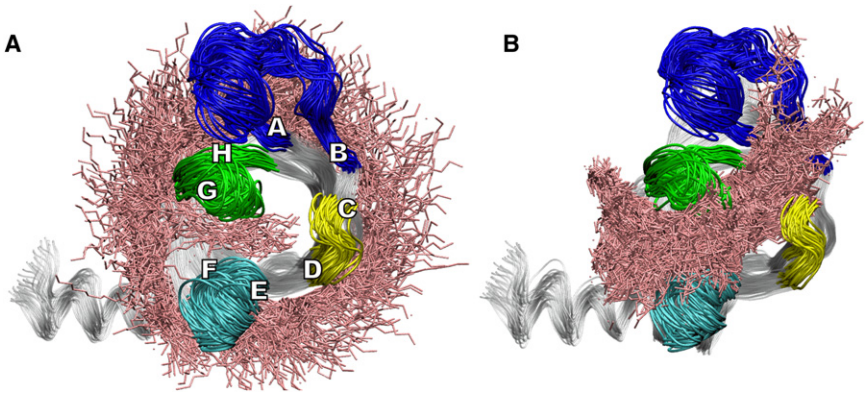

Figure 5. Plausible Routes of Ligand Entry and Exit to and from the PagP Binding Site Based on Steered MD Simulations

The strands of the β barrel are labeled A-H and the extracellular loops L1, L2, L3, and L4 are shown in dark blue, yellow, light blue, and green, respectively. Steered acyl chains are overlaid in pink. Acyl chains that jumped out of the bilayer, and all unbiased lipids, are omitted for clarity. (A) The distal 13 carbons of the *sn*-1 chain of biased POPC molecules after 1205 insertion attempts. Only the F/G route is available for insertion. (B) Detergent heavy atoms within 6 Å of PagP during 302 extraction attempts. Both the F/G and the B/C routes can be used for extraction of acyl chains from the hydrocarbon ruler pocket. See also Figure S3.

produced results similar to the simulations from the SDS structure, with additional rare phospholipid chain entry between the A and B strands (data not shown).

Gating of the F/G Crenel

In order to investigate the putative F/G route in the LDAO structure, we conducted MD simulations of the LDAO crystal structure in an explicit POPC bilayer using a nonequilibrium variant of the weighted ensemble method of Huber and Kim (1996). This evaluates the possibility of acyl-chain entry through the F/G route of the LDAO structure based on thermally driven conformational fluctuations and is conceptually similar to essential dynamics sampling (Amadei et al., 1996). In brief, the system was iteratively simulated in 0.2 ps segments, accepting simulation segments in which the donor chain spontaneously moved closer to the binding pocket, and discarding them otherwise. During this simulation, 350 of 400,000 simulation segments successfully progressed toward a bound state, yielding a biased trajectory of 70 ps. These simulations showed a disruption of the hydrogen bond between the phenolic oxygen of Tyr147 in L4 (immediately following strand G) and the amide hydrogen of Leu125 in strand F. This was followed by a rotation of the Tyr147 side chain away from strand F, opening a hole in the F/G route through which the *sn*-1 chain of the donor POPC molecule entered the PagP binding pocket (Figure 6; Movie S2). The progress of the acyl chain toward the pocket was impeded until Tyr147 moved away from Leu125. During the simulations outlined in this work, we did not observe any significant changes in the backbone H-bonding pattern of the β strands, with the exception of the Y147-L125 pair. Nevertheless, we do not rule out the possibility that such rearrangements are relevant to equilibrium binding modes.

Finally, we used functional assays to test the role of Tyr147 as a putative gating residue. Mutants Y147A and Y147F had similar CD spectra and denaturation profiles to wild-type PagP (Figures 7A and 7B), indicating that these mutations did not cause significant structural perturbations of the enzyme. PagP phospholipid:lipid A palmitoyltransferase activity was monitored in vitro using a defined detergent micellar enzymatic assay with TLC separation of radioactive lipid products (Khan et al., 2007, 2010). PagP selects the palmitate acyl chain from the phospholipid donor by a lateral lipid diffusion mechanism requiring access to the hydrocarbon ruler via the crenel located between β strands F and G (Khan and Bishop, 2009). In vitro reaction rates were measured for acylation of Kdo_2-lipid A and for the phospholipase activity. The latter assay was carried out in the absence of lipid A acceptor, in which case the rate is four to five times slower than the lipid A acylation reaction rate (Khan and Bishop, 2009). For both the acyltransferase and the phospholipase activities, the reaction rate is 2- to 3-fold faster for the Y147A and Y147F mutants relative to the wild-type (Figures 7C and 7D), suggesting a role for the phenolic hydroxyl group of tyrosine 147 in controlling phospholipid gating through the F/G crenel.

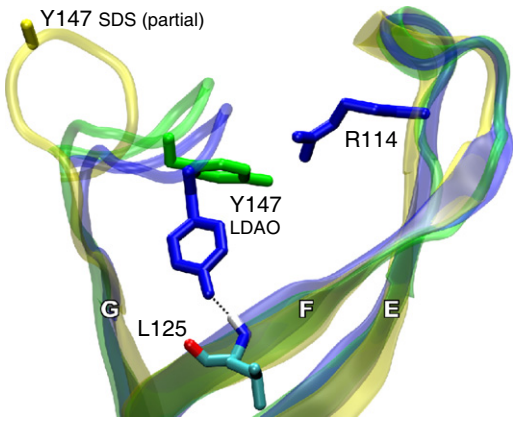

Figure 6. Side View of the Putative Ligand Entry Route at the F/G Crenel

Only PagP strands E, F, and G, including loops L3 and L4, are shown. The phenolic oxygen of Tyr147 on loop L4 makes a hydrogen bond to the backbone amide hydrogen of Leu125 and obstructs the F/G route in a MD-equilibrated structure based on the LDAO (dark blue), but not the SDS (yellow), crystal form. During nonequilibrium MD sampling based on the weighted-sampling method (shown in green), Tyr147 rotates away from strand F, allowing the *sn*-1 chain of the donor POPC molecule to enter the binding pocket (not shown). The atoms of Leu125, shown only for the MD-equilibrated structure based on the LDAO crystal form, are colored red, dark blue, light blue, and white, for oxygen, nitrogen, carbon, and hydrogen, respectively. The hydrogen bond between the Tyr147 side chains and the main chain at Leu125 is shown as a broken black line. Residue Arg114 marks the position of loop L3. See also Movie S2.

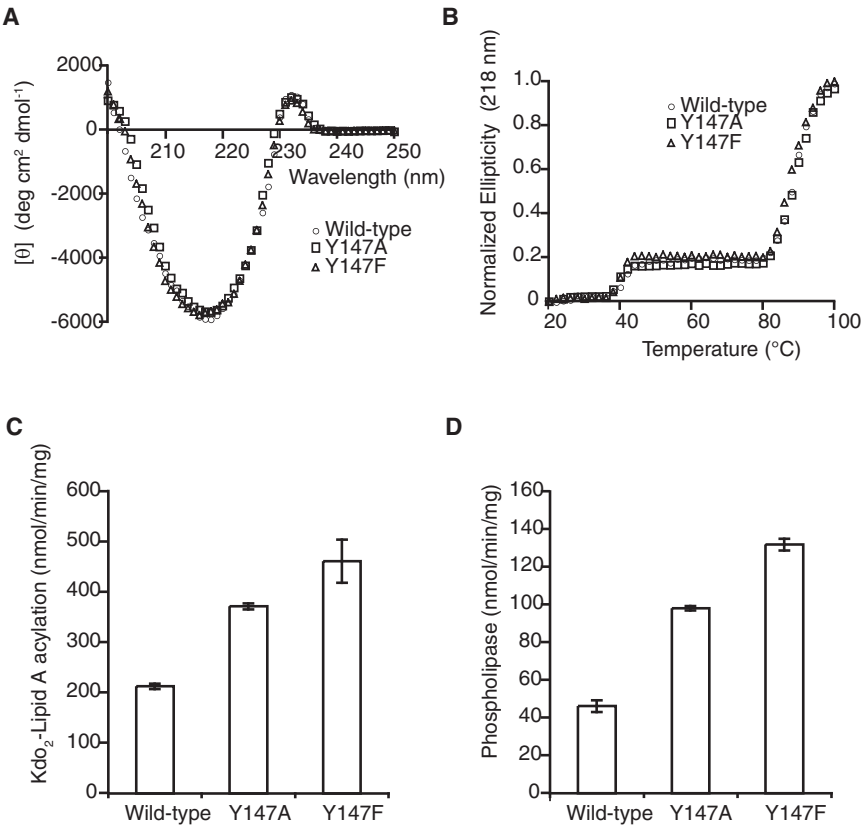

Figure 7. Analysis of Wild-type PagP and the Y147A and Y147F Mutants

Neither mutation has a significant effect on PagP structure or stability, as indicated by far UV CD spectra (A) and thermal denaturation by CD at 218 nm (B). Specific activities in vitro for lipid A palmitoyltransferase activity (C) and the phospholipase activity (D).

DISCUSSION

Crystallization from SDS/MPD

In this article, we report the use of SDS/MPD as a detergent system for membrane protein crystallization. We have previously used the SDS/MPD system to refold lysozyme (a β strand soluble protein), carbonic anhydrase (an α-helical soluble protein) and PagP (a β strand integral membrane protein) from the SDS-denatured state, indicating that the SDS/MPD system displays properties of a relatively mild detergent of wide applicability (Michaux et al., 2008a). In that study, we showed that MPD had little effect on the properties of LDAO and DM in the PagP refolding assay, and the unexpected observations were not simply due to the action of MPD on the protein. In fact, MPD is generally a mildly destabilizing osmolyte (Anand et al., 2002; Pittz and Timasheff, 1978). SDS alone has strongly denaturing properties, but the addition of MPD alters the physicochemical properties of the detergent such that the SDS micelles no longer associate strongly with polypeptides (Michaux et al., 2008a).

The mechanism of the cosolvent effect on the properties of SDS remains an area of speculation, although it is likely due to a partitioning of the cosolvent into the charged head group region of the SDS micelles thereby modifying the affinity of SDS micelles for the denatured states of the protein (Michaux et al., 2008a). The present crystal structure does not provide any insight into the SDS/MPD effect, however, since the effect depends on micellar states of the detergent. All of the ordered detergent and cosolvent molecules observed in this crystal structure associate as individual molecules with the protein surfaces, and we do not see any significant SDS-SDS or SDS-MPD interactions.

Access Route to the PagP Interior

In the structure of PagP in SDS/MPD, loops L2 and L3 have moved closer to the barrel axis relative to the LDAO structure. The largest difference, however, is the movement of loop L4 away from the acyl chain binding pocket. This creates a significant gap between strands F and G, opening a route to the internal hydrocarbon binding site. Our MD simulations are consistent in showing that this is the most favored route for acyl chain entry from the membrane phase. The increased phospholipase activity of the Tyr147 mutants provides independent experimental support that the phospholipid chain enters the barrel via the F/G route. The reaction rates for the phospholipase activity and the acyl transferase activity are affected at the same ratios by the Y147A and Y147F mutations, further suggesting that acyl chain entry is the rate limiting step in both reactions.

Additional mutants have been experimentally tested and recently reported. Hydrogen bonding between β strands F and G is disrupted by the presence of wild-type proline residues 127 and 144 which flank the PagP crenel. Mutation of each to Cys enabled crosslinking with a bifunctional reagent, which prevented the palmitoyltransferase reaction from occurring without compromising PagP structure and stability as measured by CD (Khan and Bishop, 2009). PagP has also been utilized recently as a model system to study outer membrane protein folding and assembly (Huysmans et al., 2010), and a role for weakened interstrand hydrogen bonding was suggested in identifying β barrel oligomerization interfaces (Naveed et al., 2009). Our results clearly indicate that in PagP these motifs fulfill an enzymatic role in lipid acyl chain selection.

Conclusion

A recent report on the FadL fatty acid transporter (Hearn et al., 2009) shows that hydrophobic compounds can exit this β barrel structure via a portal-type of opening in the side of the barrel wall. The structures of the FadL family of proteins are distinct from the PagP proteins, and the type of opening in the barrels is different. Nevertheless, in both cases, irregularities in the strand structures provide lateral access routes to and from the membrane hydrocarbon phase. This suggests that there are multiple ways in which β barrel membrane proteins can facilitate the passage of

hydrophobic compounds, notably acyl chains, between the bulk lipid phase and the protein interiors. The portal-type of mechanism appears to be best suited for hydrophobic ligands with small head group or no polar moieties, while the crenel-type of mechanism described here allows for lateral access of amphipathic ligands with large head groups, including bilayer-forming lipids.

EXPERIMENTAL PROCEDURES

Overexpression and Purification of PagP Inclusion Bodies

E. coli PagPΔHΔS was cloned by the Quickchange procedure (Stratagene) from the plasmids described elsewhere (Hwang et al., 2002) and expressed into inclusion bodies. BL21(DE3) cells were transformed and cell cultures were grown in LB media at 20°C until the OD_{600} reached 0.6. Expression was induced in by adding IPTG to a concentration of 0.2 mM and growth was allowed to proceed for 5 hr at 37°C. Expression of PagP is driven into inclusion bodies under these conditions. The total production of protein as inclusion bodies was approximately 1 g of PagP from 6 L of LB media in shaker flasks. The cells were lysed in an Emulsiflex cell disrupter (Avestin) and inclusion bodies were collected by centrifugation of the lysed cells. The inclusion bodies were washed three times with a buffer consisting of 2% Triton X-100 and 10 mM Tris-HCl (pH 8) followed by centrifugation at 40,000 g. The final white pellet was dissolved in 6M guanidine hydrochloride and 10 mM Tris-HCl (pH 8) for storage. A 1 ml aliquot containing 13 mg of protein was precipitated by dilution into 25 ml of 10 mM Tris-HCl (pH 8). The precipitate was washed three times by centrifugation and resuspension in 25 ml of the same buffer. No further purification steps were carried on the sample that was used for crystallization.

Refolding

The white pellet from the washed inclusion bodies (13 mg) was dissolved in 20 ml of 1% SDS, 1M MPD, and 10 mM Tris-HCl (pH 8). The solution was heated for 2 min in a boiling water bath and allowed to cool down by letting the water bath slowly return to room temperature (approximately 2 hr). Refolding proceeded virtually to completion as judged by a gel shift assay (Michaux et al., 2008a) and the presence of a positive exciton band in the CD spectra at 232 nm (Khan et al., 2007). The PagP solution was concentrated in a 10 KDa MWCO spin filter (Amicon) resulting in 1.5 ml of a solution with 5.8 mg/ml of PagP. This solution was used directly for crystallization. The protein remained folded for months under these conditions as judged by the SDS-PAGE shift assay. The SDS concentration in this stock solution was 3.8% w/v by a SDS assay (Arand et al., 1992).

Crystallization

Crystals were grown by the hanging drop method. The reservoir solution consisted of 500 μl of 1M MPD, 0.1 M Na_3Citrate buffer (pH 5.6), 1.7 M Li_2SO_4, and 0.3M $(NH_4)_2SO_4$. This mixture separates spontaneously into two phases: a hanging drop was prepared by mixing 1 μl of the lower phase (rich in salt) with 1.5 μl of the PagP stock. The hanging drop was a homogeneous mixture at first but upon equilibration with the reservoir it also separated into two phases. Crystals were obtained only in one of the two phases in the hanging drop. Crystals were allowed to grow at 20°C for 3 months and then transferred to a temperature of 4°C for 4 days. A crystal of dimensions 0.4 × 0.2 × 0.2 mm was frozen directly in its mother liquor by plunging into liquid nitrogen.

Crystallographic Data Collection

Crystallographic data were collected at the Advanced Photon Source (APS) Argonne, Illinois at beamline 19ID (λ = 0.9800 Å) on an ADSC Q315 315 × 315 mm mosaic CCD detector at a temperature of 100 K. The data were integrated and scaled with the HKL3000 package (Minor et al., 2006). The diffraction was somewhat anisotropic, and extended to a resolution of approximately 1.55 Å along the a,b directions, but strong diffraction was obtained to well beyond 1.4 Å along the c axis. Details of the solution and refinement processes are given in the Supplemental Experimental Procedures. Figures were made with Pymol (DeLano, 2002).

Structure Solution and Refinement

The structure was solved by molecular replacement using EPMR (Kissinger et al., 1999) with the structure of PagP in LDAO, PDB accession code 1THQ (Ahn et al., 2004). The structure was refined and extended using alternate cycles of manual building in Coot (Emsley and Cowtan, 2004) and refinement in Refmac5 (Murshudov et al., 1997) using the CCP4i graphical interface (Potterton et al., 2003) with implicit riding hydrogens. The stereochemical quality of the final models was assessed with MolProbity (Davis et al., 2007) and Procheck (Laskowski et al., 1993). Restraints for the MPD molecules were modified from the standard Refmac 5 dictionary by removing the torsion and chiral restraints. Restraints for the SDS molecules were adapted from Coiro and Mazza (1991). Least-squares superpositions between the different models were made with the program LSQKab (Kabsch, 1976). Only the α carbons of the residues that are in β strands in the SDS/MPD structure as indicated by Procheck were used for the superpositions (88 atoms in total). The final model had the following Ramachandran statistics for the nonglycine and nonproline residues (Laskowski et al., 1993): 88.1% in the favored regions and 9.5% in the allowed regions.

Cloning, Expression, and Refolding PagP Mutants

Wild-type PagP, and the Y147A and Y147F mutants were constructed in the pETCrcAHΔS vector, with a C-terminal His_6 tag and no signal peptide (Hwang et al., 2002) using the QuikChange protocol (Stratagene) and purified as described previously (Khan et al., 2007). The proteins were verified by electrospray ionization mass spectrometry. Precipitated protein samples were dissolved in a solution of 50:50 1% formic acid/acetonitrile just prior to ESI-MS. The sample concentration was maintained at 1 ng/μl and was injected directly onto a Waters/Micromass Q-Tof Ultima Global (a quadrupole time-of-flight) mass spectrometer. The spectra were reconstructed using MassLynx 4.0, MaxEnt 1 module. Wild-type PagP had an observed mass of 20175.3 ± 0.6 Da (theoretical mass 20175.5). Y147A PagP had an observed mass of 20082.1 ± 0.9 Da (theoretical mass 20083.4). Y147F PagP had an observed mass of 20159.5 ± 0.7 Da (theoretical mass 20159.5). The protein samples dissolved in 5 ml of 6 M Gdn-HCl, 10 mM Tris-HCl (pH 8.0) were diluted 10-fold into 10 mM Tris-HCl (pH 8.0), 0.1% LDAO. These samples were allowed to stir overnight at 4°C and applied to a NiNTA column. The samples were prepared from the columns as previously described in Khan et al. (2007). The concentration of the protein was determined using an extinction coefficient, ϵ_{280} of 80,463 M^{-1} cm^{-1} for wild-type PagP and 78,211 M^{-1} cm^{-1} for PagPY147A and PagPY147F. The extinction coefficients were determined experimentally using the Edelhoch method (Edelhoch, 1967).

In Vitro Enzymatic Assays

Kdo_2-lipid A and synthetic dipalmitoylphosphatidylcholine (DPPC) were obtained from Avanti Polar Lipids. A detailed description of the preparation of ^{32}P-labeled Kdo_2-lipid A, and thin layer chromatography (TLC)-based assays for lipid A palmitoyltransferase activity were previously described (Khan et al., 2007).

Phospholipase assays were carried out in a volume of 25 μl, with sufficient dipalmitoyl-1-^{14}C-DPPC to achieve a final concentration of 20 μM (4000 cpm/μl). The lipid was dried under a stream of N_2(g) and was dissolved in 22.5 μl reaction buffer containing 0.1M Tris-HCl (pH 8), 10 mM EDTA, and 0.25% dodecylmaltoside. The reactions were started by adding 2.5 μl of PagP and were conducted at 30°C. Reactions were stopped by adding 12.5 μl of the reaction mixture to 22.5 μl of a 1:1 $CHCl_3$/MeOH. This generated a 2-phase solution, from which 5 μl of the lower phase was spotted on a silica gel 60 plate. The experiment was carried out over 5 hr, with the reaction being spotted once every hour. TLC plates were developed in a $CHCl_3$:MeOH:H_2O (65:25:4; v/v) solvent system, which was equilibrated in sealed glass tank for 4 hr. The plates were exposed overnight to a PhosphorImager screen and developed the following day with a Molecular Dynamics Typhoon 9200 PhosphorImager.

Circular Dichroism Spectroscopy

Samples to be analyzed by CD were maintained at a concentration of 0.3 mg/ml in 10 mM Tris-HCl (pH 8.0), 0.1% LDAO and were analyzed using a cuvette of 1 mm path length. The samples were analyzed using a Aviv 215 spectropolarimeter which was linked to a Peltier device Merlin Series M25

for temperature control. For each sample, three accumulations were averaged at a data pitch of 1 nm and a scanning speed of 10 nm/min. The temperature was maintained at 25°C and data were obtained from 200 to 260 nm. Thermal denaturation profiles were obtained by heating the samples from 20°C–100°C at 218 nm with a temperature slope of 1°C/min and a response time of 3 s.

Molecular Dynamics Simulations

The simulation system consisted of a solvated POPC bilayer in which 2 PagP molecules were embedded. The binding pocket of PagP was empty for steered insertion simulations and contained a DP detergent substrate analog for steered extraction simulations. Construction and 20–50 ns equilibration of the simulation systems are described in the Supplemental Experimental Procedures.

For each molecule of PagP in each starting conformation, a separate steered insertion simulation of 100 ps was carried out in which the *sn-1* chain of a single phospholipid in the upper bilayer leaflet was forced toward the PagP binding pocket with a force of constant magnitude. Phospholipids were targeted for insertion if at least one of the distal 13 carbons in the *sn-1* chain was within 3 nm of the protein. Similarly, steered extraction simulations forced the DP molecule away from its initial position in the PagP binding pocket. Additional details are provided in the Supplemental Experimental Procedures.

The Berger parameters (Berger et al., 1997) for POPC (Tieleman et al., 1998) and the OPLSAA parameters (Kaminski et al., 2001) for PagP were properly combined for the GROMACS simulation package (Lindahl et al., 2001) using the half-ε double-pairlist method (Chakrabarti et al., 2010) (Figure S3). In brief, the ε values of the 1-4 Lennard-Jones parameters of the lipids were multiplied by an additional factor of 0.5 in the pair-types section and the list of 1–4 interactions in the pairs section was duplicated. The regular OPLSAA combination rules were then applied. Additional details are provided in Supplemental Experimental Procedures and Figure S3.

ACCESSION NUMBERS

Atomic coordinates and structure factors have been deposited in the PDB (http://www.rcsb.org) under the accession code 3GP6.

SUPPLEMENTAL INFORMATION

Supplemental Information includes Supplemental Experimental Procedures, three figures, and two movies and can be found with this article online at doi:10.1016/j.str.2010.06.014.

ACKNOWLEDGMENTS

G.G.P. was supported by CIHR operating grant MOP-13335 and IG1-93473. J.A.C.-S was supported by the CIHR Training Program in the Structural Biology of Membrane Proteins Linked to Disease. Computational studies were made possible by the facilities of the Centre for Computational Biology High Performance Facility (CCBHPF) at the Hospital for Sick Children and the Shared Hierarchical Academic Research Computing Network (SHARCNET). C.N. acknowledges support from the Research Training Centre at the Hospital for Sick Children and from the University of Toronto. R.P. is a CRCP chairholder and is supported by CIHR operating grant MOP-43998. Work in the laboratory of R.E.B. is supported by CIHR operating grant MOP-84329. This research was funded in part by the Ontario Ministry of Health and Long Term Care. The views expressed do not necessarily reflect those of the OMOHLTC.

Received: September 8, 2009
Revised: May 31, 2010
Accepted: June 7, 2010
Published: September 7, 2010

REFERENCES

Ahn, V.E., Lo, E.I., Engel, C.K., Chen, L., Hwang, P.M., Kay, L.E., Bishop, R.E., and Privé, G.G. (2004). A hydrocarbon ruler measures palmitate in the enzymatic acylation of endotoxin. EMBO J. *23*, 2931–2941.

Amadei, A., Linssen, A.B., de Groot, B.L., van Aalten, D.M., and Berendsen, H.J. (1996). An efficient method for sampling the essential subspace of proteins. J. Biomol. Struct. Dyn. *13*, 615–625.

Anand, K., Pal, D., and Hilgenfeld, R. (2002). An overview on 2-methyl-2,4-pentanediol in crystallization and in crystals of biological macromolecules. Acta Crystallogr. D Biol. Crystallogr. *58*, 1722–1728.

Arand, M., Friedberg, T., and Oesch, F. (1992). Colorimetric quantitation of trace amounts of sodium lauryl sulfate in the presence of nucleic acids and proteins. Anal. Biochem. *207*, 73–75.

Bader, M.W., Sanowar, S., Daley, M.E., Schneider, A.R., Cho, U., Xu, W., Klevit, R.E., Le Moual, H., and Miller, S.I. (2005). Recognition of antimicrobial peptides by a bacterial sensor kinase. Cell *122*, 461–472.

Berger, O., Edholm, O., and Jahnig, F. (1997). Molecular dynamics simulations of a fluid bilayer of dipalmitoylphosphatidylcholine at full hydration, constant pressure, and constant temperature. Biophys. J. *72*, 2002–2013.

Bishop, R.E. (2005). The lipid A palmitoyltransferase PagP: molecular mechanisms and role in bacterial pathogenesis. Mol. Microbiol. *57*, 900–912.

Bishop, R.E., Gibbons, H.S., Guina, T., Trent, M.S., Miller, S.I., and Raetz, C.R. (2000). Transfer of palmitate from phospholipids to lipid A in outer membranes of gram-negative bacteria. EMBO J. *19*, 5071–5080.

Chakrabarti, N., Neale, C., Payandeh, J., Pai, E.F., and Pomés, R. (2010). An iris-like mechanism of pore dilation in the CorA magnesium transport system. Biophys. J. *98*, 784–792.

Cherezov, V., Yamashita, E., Liu, W., Zhalnina, M., Cramer, W.A., and Caffrey, M. (2006). In meso structure of the cobalamin transporter, BtuB, at 1.95 A resolution. J. Mol. Biol. *364*, 716–734.

Coiro, V., and Mazza, F. (1991). Crystal phases of dodecyl sulfates obtained from aqueous solutions: structure of the hexaaquamagnesium salt. Crystal Structure Communications *47*, 1169–1173.

Cox, K., and Sansom, M.S. (2009). One membrane protein, two structures and six environments: a comparative molecular dynamics simulation study of the bacterial outer membrane protein PagP. Mol. Membr. Biol. *26*, 205–214.

Davis, I.W., Leaver-Fay, A., Chen, V.B., Block, J.N., Kapral, G.J., Wang, X., Murray, L.W., Arendall, W.B., 3rd, Snoeyink, J., Richardson, J.S., and Richardson, D.C. (2007). MolProbity: all-atom contacts and structure validation for proteins and nucleic acids. Nucleic Acids Res. *35*, W375–W383. doi: 10.1093/nar/gkm216.

DeLano, W.L. (2002). The PyMOL Molecular Graphics System.

Edelhoch, H. (1967). Spectroscopic determination of tryptophan and tyrosine in proteins. Biochemistry *6*, 1948–1954.

Emsley, P., and Cowtan, K. (2004). Coot: model-building tools for molecular graphics. Acta Crystallogr. D Biol. Crystallogr. *60*, 2126–2132.

Evanics, F., Hwang, P.M., Cheng, Y., Kay, L.E., and Prosser, R.S. (2006). Topology of an outer-membrane enzyme: Measuring oxygen and water contacts in solution NMR studies of PagP. J. Am. Chem. Soc. *128*, 8256–8264.

Guo, L., Lim, K.B., Poduje, C.M., Daniel, M., Gunn, J.S., Hackett, M., and Miller, S.I. (1998). Lipid A acylation and bacterial resistance against vertebrate antimicrobial peptides. Cell *95*, 189–198.

Guo, X.H., Zhao, N.M., Chen, S.H., and Teixeira, J. (1990). Small-angle neutron scattering study of the structure of protein/detergent complexes. Biopolymers *29*, 335–346.

Hearn, E.M., Patel, D.R., Lepore, B.W., Indic, M., and van den Berg, B. (2009). Transmembrane passage of hydrophobic compounds through a protein channel wall. Nature *458*, 367–370.

Heaslet, H., Rosenfeld, R., Giffin, M., Lin, Y.C., Tam, K., Torbett, B.E., Elder, J.H., McRee, D.E., and Stout, C.D. (2007). Conformational flexibility in the flap domains of ligand-free HIV protease. Acta Crystallogr. D Biol. Crystallogr. *63*, 866–875.

Helenius, A., and Simons, K. (1975). Solubilization of membranes by detergents. Biochim. Biophys. Acta *415*, 29–79.

Huber, G.A., and Kim, S. (1996). Weighted-ensemble Brownian dynamics simulations for protein association reactions. Biophys. J. *70*, 97–110.

Hunte, C., and Richers, S. (2008). Lipids and membrane protein structures. Curr. Opin. Struct. Biol. *18*, 406–411.

Huysmans, G.H., Radford, S.E., Brockwell, D.J., and Baldwin, S.A. (2007). The N-terminal helix is a post-assembly clamp in the bacterial outer membrane protein PagP. J. Mol. Biol. *373*, 529–540.

Huysmans, G.H., Baldwin, S.A., Brockwell, D.J., and Radford, S.E. (2010). The transition state for folding of an outer membrane protein. Proc. Natl. Acad. Sci. USA *107*, 4099–4104.

Hwang, P.M., Choy, W.Y., Lo, E.I., Chen, L., Forman-Kay, J.D., Raetz, C.R., Privé, G.G., Bishop, R.E., and Kay, L.E. (2002). Solution structure and dynamics of the outer membrane enzyme PagP by NMR. Proc. Natl. Acad. Sci. USA *99*, 13560–13565.

Hwang, P.M., Bishop, R.E., and Kay, L.E. (2004). The integral membrane enzyme PagP alternates between two dynamically distinct states. Proc. Natl. Acad. Sci. USA *101*, 9618–9623.

Jia, W., El Zoeiby, A., Petruzziello, T.N., Jayabalasingham, B., Seyedirashti, S., and Bishop, R.E. (2004). Lipid trafficking controls endotoxin acylation in outer membranes of Escherichia coli. J. Biol. Chem. *279*, 44966–44975.

Kabsch, W. (1976). A solution for the best rotation to relate two sets of vectors. Acta Cryst. *A32*, 922–923.

Kaminski, G., Friesner, R., Tirado-Rives, J., and Jorgensen, W. (2001). Evaluation and Reparametrization of the OPLS-AA Force Field for Proteins via Comparison with Accurate Quantum Chemical Calculations on Peptides. J. Phys. Chem. B *105*, 6474–6487.

Kawasaki, K., Ernst, R.K., and Miller, S.I. (2004). 3-O-deacylation of lipid A by PagL, a PhoP/PhoQ-regulated deacylase of Salmonella typhimurium, modulates signaling through Toll-like receptor 4. J. Biol. Chem. *279*, 20044–20048.

Khan, M.A., and Bishop, R.E. (2009). Molecular mechanism for lateral lipid diffusion between the outer membrane external leaflet and a beta-barrel hydrocarbon ruler. Biochemistry *48*, 9745–9756.

Khan, M.A., Neale, C., Michaux, C., Pomès, R., Privé, G.G., Woody, R.W., and Bishop, R.E. (2007). Gauging a hydrocarbon ruler by an intrinsic exciton probe. Biochemistry *46*, 4565–4579.

Khan, M.A., Moktar, J., Mott, P.J., and Bishop, R.E. (2010). A thiolate anion buried within the hydrocarbon ruler perturbs PagP lipid acyl chain selection. Biochemistry *49*, 2368–2379.

Kissinger, C.R., Gehlhaar, D.K., and Fogel, D.B. (1999). Rapid automated molecular replacement by evolutionary search. Acta Crystallogr. D Biol. Crystallogr. *55*, 484–491.

Laskowski, R.A., MacArthur, M.W., Moss, D.S., and Thornton, J.M. (1993). PROCHECK: a program to check the stereochemical quality of protein structures. J. Appl. Crystallogr. *26*, 283–291.

Lindahl, E., Hess, B., and van der Spoel, D. (2001). GROMACS 3.0: a package for molecular simulation and trajectory analysis. J. Mol. Model. *7*, 306–317.

Manning, M., and Colon, W. (2004). Structural basis of protein kinetic stability: resistance to sodium dodecyl sulfate suggests a central role for rigidity and a bias toward beta-sheet structure. Biochemistry *43*, 11248–11254.

Mattice, W.L., Riser, J.M., and Clark, D.S. (1976). Conformational properties of the complexes formed by proteins and sodium dodecyl sulfate. Biochemistry *15*, 4264–4272.

Michaux, C., Pomroy, N.C., and Privé, G.G. (2008a). Refolding SDS-denatured proteins by the addition of amphipathic cosolvents. J. Mol. Biol. *375*, 1477–1488.

Michaux, C., Pouyez, J., Wouters, J., and Privé, G.G. (2008b). Protecting role of cosolvents in protein denaturation by SDS: a structural study. BMC Struct. Biol. *8*, 29.

Minor, W., Cymborowski, M., Otwinowski, Z., and Chruszcz, M. (2006). HKL-3000: the integration of data reduction and structure solution–from diffraction images to an initial model in minutes. Acta Crystallogr. D Biol. Crystallogr. *62*, 859–866.

Muroi, M., Ohnishi, T., and Tanamoto, K. (2002). MD-2, a novel accessory molecule, is involved in species-specific actions of Salmonella lipid A. Infect. Immun. *70*, 3546–3550.

Murshudov, G.N., Vagin, A.A., and Dodson, E.J. (1997). Refinement of macromolecular structures by the maximum-likelihood method. Acta Crystallogr. D Biol. Crystallogr. *53*, 240–255.

Naveed, H., Jackups, R., Jr., and Liang, J. (2009). Predicting weakly stable regions, oligomerization state, and protein-protein interfaces in transmembrane domains of outer membrane proteins. Proc. Natl. Acad. Sci. USA *106*, 12735–12740.

Nielsen, M.M., Andersen, K.K., Westh, P., and Otzen, D.E. (2007). Unfolding of beta-sheet proteins in SDS. Biophys. J. *92*, 3674–3685.

Otzen, D.E. (2002). Protein unfolding in detergents: effect of micelle structure, ionic strength, pH, and temperature. Biophys. J. *83*, 2219–2230.

Otzen, D.E., and Oliveberg, M. (2002). Burst-phase expansion of native protein prior to global unfolding in SDS. J. Mol. Biol. *315*, 1231–1240.

Pilione, M.R., Pishko, E.J., Preston, A., Maskell, D.J., and Harvill, E.T. (2004). pagP is required for resistance to antibody-mediated complement lysis during Bordetella bronchiseptica respiratory infection. Infect. Immun. *72*, 2837–2842.

Pittz, E.P., and Timasheff, S.N. (1978). Interaction of ribonuclease A with aqueous 2-methyl-2,4-pentanediol at pH 5.8. Biochemistry *17*, 615–623.

Potterton, E., Briggs, P., Turkenburg, M., and Dodson, E. (2003). A graphical user interface to the CCP4 program suite. Acta Crystallogr. D Biol. Crystallogr. *59*, 1131–1137.

Preston, A., Maxim, E., Toland, E., Pishko, E.J., Harvill, E.T., Caroff, M., and Maskell, D.J. (2003). Bordetella bronchiseptica PagP is a Bvg-regulated lipid A palmitoyl transferase that is required for persistent colonization of the mouse respiratory tract. Mol. Microbiol. *48*, 725–736.

Privé, G.G. (2007). Detergents for the stabilization and crystallization of membrane proteins. Methods *41*, 388–397.

Qin, L., Hiser, C., Mulichak, A., Garavito, R.M., and Ferguson-Miller, S. (2006). Identification of conserved lipid/detergent-binding sites in a high-resolution structure of the membrane protein cytochrome c oxidase. Proc. Natl. Acad. Sci. USA *103*, 16117–16122.

Raetz, C.R., Reynolds, C.M., Trent, M.S., and Bishop, R.E. (2007). Lipid A modification systems in gram-negative bacteria. Annu. Rev. Biochem. *76*, 295–329.

Raman, P., Cherezov, V., and Caffrey, M. (2006). The Membrane Protein Data Bank. Cell. Mol. Life Sci. *63*, 36–51.

Reynolds, J.A., and Tanford, C. (1970). The gross conformation of protein-sodium dodecyl sulfate complexes. J. Biol. Chem. *245*, 5161–5165.

Robey, M., O'Connell, W., and Cianciotto, N.P. (2001). Identification of Legionella pneumophila rcp, a pagP-like gene that confers resistance to cationic antimicrobial peptides and promotes intracellular infection. Infect. Immun. *69*, 4276–4286.

Samso, M., Daban, J.R., Hansen, S., and Jones, G.R. (1995). Evidence for sodium dodecyl sulfate/protein complexes adopting a necklace structure. Eur. J. Biochem. *232*, 818–824.

Smith, B.J. (1994). SDS polyacrylamide gel electrophoresis of proteins. Methods Mol. Biol. *32*, 23–34.

Smith, A.E., Kim, S.H., Liu, F., Jia, W., Vinogradov, E., Gyles, C.L., and Bishop, R.E. (2008). PagP activation in the outer membrane triggers R3 core oligosaccharide truncation in the cytoplasm of Escherichia coli O157:H7. J. Biol. Chem. *283*, 4332–4343.

Snijder, H.J., Van Eerde, J.H., Kingma, R.L., Kalk, K.H., Dekker, N., Egmond, M.R., and Dijkstra, B.W. (2001). Structural investigations of the active-site mutant Asn156Ala of outer membrane phospholipase A: function of the Asn-His interaction in the catalytic triad. Protein Sci. *10*, 1962–1969.

Tanamoto, K., and Azumi, S. (2000). Salmonella-type heptaacylated lipid A is inactive and acts as an antagonist of lipopolysaccharide action on human line cells. J. Immunol. *164*, 3149–3156.

Tieleman, D.P., Forrest, L.R., Sansom, M.S., and Berendsen, H.J. (1998). Lipid properties and the orientation of aromatic residues in OmpF, influenza M2, and alamethicin systems: molecular dynamics simulations. Biochemistry *37*, 17554–17561.

Vandeputte-Rutten, L., Kramer, R.A., Kroon, J., Dekker, N., Egmond, M.R., and Gros, P. (2001). Crystal structure of the outer membrane protease OmpT from Escherichia coli suggests a novel catalytic site. EMBO J. *20*, 5033–5039.

Structure *18*

Supplemental Information

PagP Crystallized from SDS/Cosolvent Reveals the Route for Phospholipid Access to the Hydrocarbon Ruler

Jose Antonio Cuesta-Seijo, Chris Neale, M. Adil Khan, Joel Moktar, Christopher Tran, Russell E Bishop, Régis Pomès, and Gilbert G. Privé

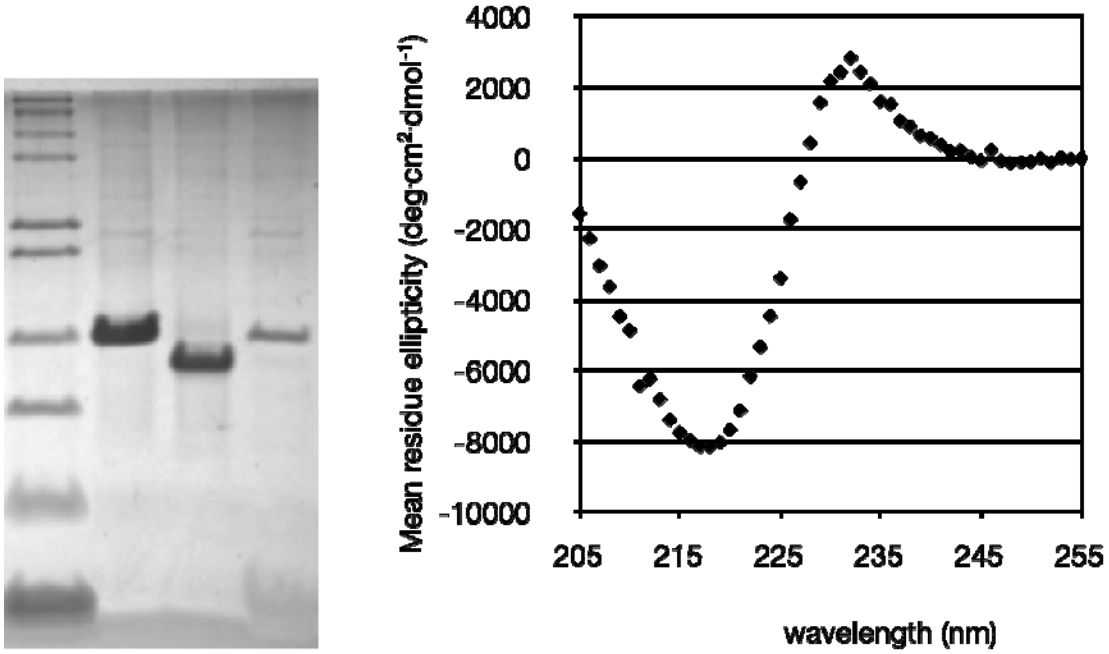

Figure S1, related to Figure 2. Refolding of PagP in SDS/MPD

Left. 18% SDS-PAGE of the protein crystallization stock. From left to right, Mark 12 molecular weight standards, 1 μL of the crystallization protein stock, 5 μg of PagP unfolded in SDS alone and 2 μg of PagP folded in LDAO. The gel was stained with Simply Blue (Invtrogen).

Right. CD spectrum of the sample prior to the concentration step (see Methods). The maximum at 232 nm is indicative of the correct formation of the hydrocarbon ruler, the minimum at 218 nm of the β–sheet structure.

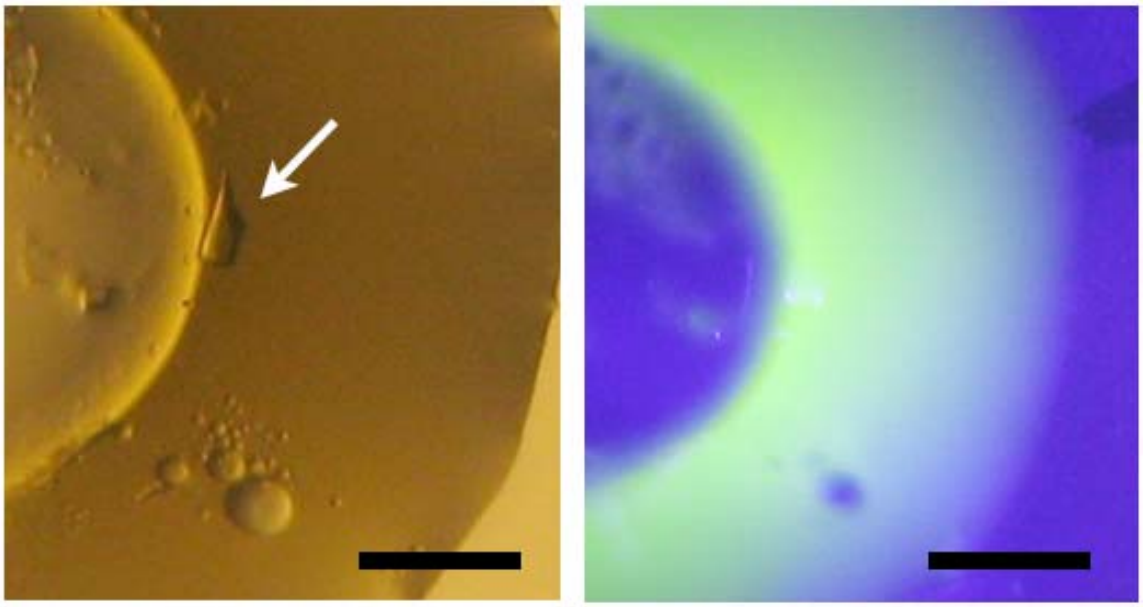

Figure S2, related to Figure 3. PagP crystals grow from a SDS-rich phase
Left: Phase separation and crystallization of PagP from SDS/MPD. The white arrow indicates a PagP crystal. Right: The same droplet after the addition of the fluorescent lipid NBD-DPPC and viewed under UV light. The lipid partitions into the phase that contains the crystal, as seen by the green fluorescence. The scale bar represents 100 μm.

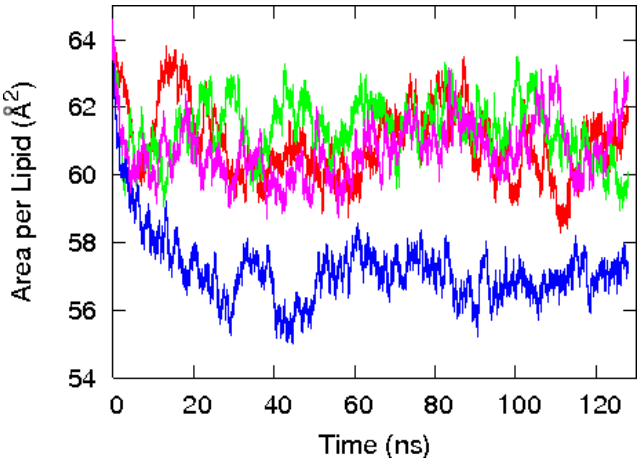

Figure S3, related to Figure 5.
The area per lipid time series at 323K for simulations employing the forcefield parameters of (red) standard ffgmx, (green) ffgmx converted to ε and δ, (blue) unmodified ε and δ using OPLSAA scaling rules, (purple) the half-ε double-pairlist method for combination with OPLSAA.

SUPPLEMENTAL EXPERIMENTAL PROCEDURES

Molecular Dynamics Simulations

Simulation conditions. Simulations were conducted with version 3.3.1 of the GROMACS simulation package (Lindahl et al., 2001), modified to apply a biasing force of constant magnitude. The Berger parameters (Berger et al., 1997) for POPC (Tieleman et al., 1998) and the OPLSAA parameters (Kaminski et al., 2001) for PagP were combined using the half-ε double-pairlist method (Chakrabarti et al., 2010). The water model was TIP4P (Jorgensen et al., 1983). Periodic boundary conditions were enforced via a rectangular unit cell. Lennard–Jones interactions were evaluated using a group-based twin-range cutoff (van Gunsteren and Berendsen, 1990) calculated every step for separation distances less than 0.9 nm and every ten steps for distances between 0.9 and 1.4 nm, when the nonbonded list was updated. Coulomb interactions were calculated using the smooth particle-mesh Ewald method (Darden et al., 1993; Essmann et al., 1995) with a real-space cutoff of 0.9 nm and a Fourier grid spacing of 0.12 nm. Simulation in the *NpT* ensemble was achieved by isotropic coupling to a Berendsen barostat (Berendsen et al., 1984) at 1 bar with a coupling constant of 4 ps and separate coupling of the solute and the solvent to Berendsen thermostats (Berendsen et al., 1984) at 310 K with coupling constants of 0.1 ps. Bonds involving hydrogen were constrained with SETTLE (Miyamoto and Kollman, 1992) and LINCS (Hess et al., 1997) for solvent and solute, respectively. The integration time step was 2 fs.

POPC bilayer construction. A POPC molecule was constructed based on the 1,2-dilauryl-*sn*-glycero-3-phosphoethanolamine (DLPE) crystal structure of Elder et al. (Elder et al., 1977) by replacing amide hydrogens with methyls and extending the acyl chains in the *trans* conformation. A POPC bilayer with 160 lipids per leaflet measuring 7.77 nm by 7.96 nm in the bilayer plane was then constructed based on the DLPE crystal

symmetry (Elder et al., 1977). The rectangular unit cell was set to 20 nm normal to the plane of the bilayer and solvated with 29,953 TIP4P water molecules. The crystal symmetry was broken using a protocol derived from Takaoka *et al.* (Takaoka et al., 2000). However, we found that a preliminary low temperature simulation was required to prevent leaflet separation during the 510 K pulse, and that a large excess of water normal to the bilayer was required to accommodate undulations that were induced when, at 510 K, the area per lipid increased more quickly than could be accommodated in the bilayer plane by pressure coupling. Our protocol was 0-1 ns: 310 K, 1-1.1 ns: gradual heating to 510 K, 1.1-1.17 ns: gradual cooling to 360 K, 1.17-5.17 ns: 360 K, 5.17-40 ns: 323 K. At this point, the system dimensions were 10.4 nm by 9.8 nm in the bilayer plane and 12 nm along the bilayer normal. The undulations had reduced significantly by this point and we reduced the unit cell to 8 nm along the bilayer normal, excluding a large number of water molecules. This smaller system was simulated for an additional 50 ns at 310 K. A time-dependent analysis of the order parameters of the acyl chains indicated that the bulk properties of the bilayer had converged after 25 ns (not shown). The coordinates of this bilayer at 25 ns were used for the study of PagP.

*PagP all-atom modelling***.** The available coordinates for PagP, including crystal waters within 5 Å, were taken from the crystal structure presented in this article. We then constructed 1000 candidate models of L1 loop residues 38-45 as random coil using the program Loopy (Xiang et al., 2002), keeping the two loop conformations of lowest colony energy. To both of these structures, we modelled the missing sidechains for residues 4, 35, 36, 38-45, 46, 47, 146, 147, and 148 with SCWRL 3.0 (Canutescu et al., 2003), during which we found it necessary to manually direct Y46 $\chi 1$ to -120˚ to avoid atomic overlap. A single molecule of dodecyl phosphate (DP) was placed in the PagP binding pocket as a dodecyl sulphate analog. Parameters for DP were constructed based on those of dodecyl phosphocholine (DPC) (Tieleman et al., 2000) by removing the choline group and adding a partial charge of 0.1 to each of the four oxygens.

Composite system creation. Two copies of PagP having different L1 loop conformations were overlaid on the POPC bilayer with the principle axis of each β-barrel oriented 15° to the bilayer normal, bringing the L3 loop toward the bilayer, in order to align the exposed hydrophobic/hydrophilic surfaces with the hydrophobicity profile of the bilayer as suggested by Ahn *et al.* (Ahn et al., 2004). To reduce any anisotropic effects that the mobile loop regions of the protein may inflict upon the relative surface tension of each leaflet, the proteins were inserted anti-parallel to one another. Any phospholipid within 0.2 Å was removed, additionally removing a minimal number of phospholipids while ensuring that each leaflet contained the same amount. A surface representation of each protein was then constructed using MSMS (Sanner et al., 1996) and PagP-shaped holes were made in the bilayer according to the protocol of Faraldo-Gomez *et al.* (Faraldo-Gomez et al., 2002) in 3 segments of 20 ps each while applying a position restraint along the bilayer normal with a force constant of 1000 kJ mol^{-1} nm^{-2} on phosphorous atoms of all lipids. The strength of the hole-making force was 10, 100, and 500 kJ mol^{-1} nm^{-2} in the first, second and third segments, respectively. The composite system, composed of a solvated POPC bilayer, two protein molecules and associated DP and crystal waters, was neutralized with 8 Na^{+} ions and simulated for 50 ns at 310 K, with the position of protein and DP heavy atoms restrained during the first 5 ns. The rate at which the backbone RMSD to the crystal structure increased was significantly attenuated by 15 ns (not shown), and hence the final 30 ns of this simulation was used to generate conformations with which to initiate non-equilibrium steered MD simulations. Starting configurations for steered insertion of the *sn-1* chain of a POPC molecule into the PagP binding pocket and steered extraction of a DP molecule from the PagP binding

pocket were taken at 2 ns and 200 ps intervals, respectively. Prior to the initiation of steered insertion simulations, both DP molecules and two Na^+ ions were removed from the system.

Steered MD simulations. Steered insertion simulations employed a constant magnitude biasing force of the form

$$F = \frac{-K}{\left| x^{ligand} - x^{ref} \right|}(x^{ligand} - x^{ref}) \qquad (1)$$

where x_{ligand} represents the current position of the centre of mass of the distal 13 carbons in the *sn-1* chain of the selected phospholipid and x_{ref} represents the reference position calculated as

$$x^{ref} = x^{PagP} + x_0^{DP} + x_0^{PagP} \qquad (2)$$

in which the current position of the centre of mass of the PagP β-barrel, x^{PagP}, is offset by the vector from the initial center of mass of the PagP β-barrel, x_0^{PagP}, to the initial centre of mass of the DP molecule that was removed from the binding pocket, x_0^{DP}. Only biasing force components in the bilayer plane were applied. The constant K was set to 500 kJ mol^{-1} nm^2 such that the targeted *sn-1* chain is attracted to the PagP binding pocket. For steered extraction simulations, x^{ligand} represents the current position of the centre of mass of DP and the constant K was set to -500 kJ mol^{-1} nm^2 such that DP is repelled from its initial position.

The 100-ps length of the simulations is sufficient to observe productive insertions, yet short enough to allow a large number of repeats (1507 in this work) for the sake of statistical significance. In addition, the applied force should be large enough to promote a significant number of productive insertions yet small enough to ensure a significant number of unsuccessful attempts; furthermore, the latter should not perturb the protein structure significantly. With this in mind, we conducted preliminary simulations with three different force constants of 100, 500, and 1000 $kJ \cdot mol^{-1} \cdot nm^{-2}$ (results not shown), based on which we selected 500 $kJ \cdot mol^{-1} \cdot nm^{-2}$.

Half-ε double-pairlist combination rules for Berger lipids and OPLSAA proteins. During MD simulation, non-bonded interactions between atoms that are separated by exactly three bonds (the so-called 1-4 interactions) are often scaled by some factor from their full strength. This scaling factor differs amongst forcefields and thus the simultaneous use of multiple forcefields requires special attention to ensure that the 1-4 interactions of all molecules are properly scaled. Indeed, combination of the Berger lipid parameters and the OPLSAA protein parameters within the molecular dynamics simulation package GROMACS is complicated by the inability to specify unique parameters for Coulombic 1-4 interactions. It is this deficiency that led Tieleman *et al.* (Tieleman et al., 2006) to reparametrize the dihedral angle energy functions of the Berger lipids such that the nonbonded component of the 1-4 interactions is accounted for by the new dihedral potentials. While the published reparametrization of dihedral parameters appears to be a valid solution, one would like to avoid reparametrizing every lipid and detergent for which parameters have already been generated using this lipid forcefield. To this end, we apply a simple method that can be used within GROMACS to combine the above-mentioned forcefields while properly scaling the 1-4 nonbonded interactions of each that is at once simpler and more inclusive. This method makes use of the fact that (i) it is possible to specify a unique value for the LJ component of the 1-4 interactions, and

(ii) the scaling factor for the Coulombic component of the 1-4 interactions of one forcefield is an integer multiple of the scaling factor used in the other forcefield (1.0 for Berger lipids and 0.5 for OPLSAA). Specifically, in the GROMACS topology file, the ε values of the 1-4 LJ parameters of the lipids are multiplied by an additional factor of 0.5 in the pairtypes section and the list of 1-4 interactions in the pairs section is duplicated. The regular OPLSAA combination rules are then applied. In this way, the LJ and Coulombic 1-4 interactions are both cut in half and then included twice for the lipids, yielding properly scaled 1-4 interactions for both Berger lipids and OPLSAA protein. This method is referred to as the half-ε double-pairlist method (Chakrabarti et al., 2010).

Supplemental Figure S3 shows the area per lipid obtained from simulating a bilayer composed of 1,2-dipalmitoyl-*sn*-glycero-3-phosphocholine (DPPC), containing 64 lipids per leaflet solvated by 28.5 SPC (Berendsen et al., 1981) waters per lipid, using a variety of methods to treat the lipid forcefield. Initial DPPC parameters were taken from Tieleman et al. (Tieleman and Berendsen, 1996). The area per lipid derived from the direct use of lipid.itp and ffgmx, a forcefield that does not arbitrarily scale 1-4 interactions, is traced by the red line. Similar results are found when the functional form of the LJ variables are converted from C6/C12 to δ/ε while leaving 1-4 interactions as intended (blue line) and when applying the half-ε double-pairlist method under the OPLSAA scaling rules (purple line). However, the area per lipid is significantly reduced when the unmodified δ/ε formulation of LJ interactions is used while scaling lipid 1-4 interactions according to the rules of OPLSAA (blue line). In this set of conditions, the Coulombic 1-4 interactions of lipids are erroneously assigned only half of their full strength.

SUPPLEMENTAL REFERENCES

Ahn, V.E., Lo, E.I., Engel, C.K., Chen, L., Hwang, P.M., Kay, L.E., Bishop, R.E., and Privé, G.G. (2004). A hydrocarbon ruler measures palmitate in the enzymatic acylation of endotoxin. EMBO J *23*, 2931-2941.

Berendsen, H., Postma, J., van Gunsteren, W., DiNola, A., and Haak, J. (1984). Molecular dynamics with coupling to an external bath. The Journal of Chemical Physics *81*, 3684.

Berendsen, H., Postma, J., van Gunsteren, W., and Hermans, J. (1981). Interaction models for water in relation to protein hydration. In Intermolecular Forces, B. Pullman, ed. (Dordrecht, The Netherlands: Reidel), pp. 331-342.

Berger, O., Edholm, O., and Jahnig, F. (1997). Molecular dynamics simulations of a fluid bilayer of dipalmitoylphosphatidylcholine at full hydration, constant pressure, and constant temperature. Biophys J *72*, 2002-2013.

Canutescu, A.A., Shelenkov, A.A., and Dunbrack, R.L., Jr. (2003). A graph-theory algorithm for rapid protein side-chain prediction. Protein Sci *12*, 2001-2014.

Chakrabarti, N., Neale, C., Payandeh, J., Pai, E.F., and Pomes, R. (2010). An iris-like mechanism of pore dilation in the CorA magnesium transport system. Biophys J *98*, 784-792.

Darden, T., York, D., and Pedersen, L. (1993). Particle mesh Ewald: An N+log(N) method for Ewald sums in large systems. Journal of Chemical Physics *98*, 10089-10092.

Elder, M., Hitchcock, P., Mason, R., and Shipley, G. (1977). A Refinement Analysis of the Crystallography of the Phospholipid, 1, 2-Dilauroyl-DL-Phosphatidylethanolamine, and Some Remarks on Lipid-Lipid and Lipid-Protein Interactions. Proceedings of the

Royal Society of London. Series A, Mathematical and Physical Sciences (1934-1990) *354*, 157-170.
Essmann, U., Perera, L., Berkowitz, M., Darden, T., Lee, H., and Pedersen, L. (1995). A smooth particle mesh Ewald method. The Journal of Chemical Physics *103*, 8577.
Faraldo-Gomez, J.D., Smith, G.R., and Sansom, M.S. (2002). Setting up and optimization of membrane protein simulations. Eur Biophys J *31*, 217-227.
Hess, B., Bekker, H., Berendsen, H., and Fraaije, J. (1997). J. Comput. Chem. *18*, 1463-1472.
Jorgensen, W., Chandrasekhar, J., Madura, J., Impey, R., and Klein, M. (1983). Comparison of simple potential functions for simulating liquid water. The Journal of Chemical Physics *79*, 926.
Kaminski, G., Friesner, R., Tirado-Rives, J., and Jorgensen, W. (2001). Evaluation and Reparametrization of the OPLS-AA Force Field for Proteins via Comparison with Accurate Quantum Chemical Calculations on Peptides. Journal of Physical Chemistry B *105*, 6474-6487.
Lindahl, E., Hess, B., and van der Spoel, D. (2001). GROMACS 3.0: a package for molecular simulation and trajectory analysis. Journal of Molecular Modeling *7*, 306-317.
Miyamoto, S., and Kollman, P. (1992). Settle: An analytical version of the SHAKE and RATTLE algorithm for rigid water models. Journal of Computational Chemistry *13*, 952-962.
Sanner, M.F., Olson, A.J., and Spehner, J.C. (1996). Reduced surface: an efficient way to compute molecular surfaces. Biopolymers *38*, 305-320.
Takaoka, Y., Pasenkiewicz-Gierula, M., Miyagawa, H., Kitamura, K., Tamura, Y., and Kusumi, A. (2000). Molecular Dynamics Generation of Nonarbitrary Membrane Models Reveals Lipid Orientational Correlations. Biophysical Journal *79*, 3118-3138.
Tieleman, D., and Berendsen, H. (1996). Molecular dynamics simulations of a fully hydrated dipalmitoylphosphatidylcholine bilayer with different macroscopic boundary conditions and parameters. The Journal of Chemical Physics *105*, 4871.
Tieleman, D., MacCallum, J., Ash, W., Kandt, C., Xu, Z., and Monticelli, L. (2006). Membrane protein simulations with a united-atom lipid and all-atom protein model: lipid-protein interactions, side chain transfer free energies and model proteins. JOURNAL OF PHYSICS CONDENSED MATTER *18*, 1221.
Tieleman, D., van der Spoel, D., and Berendsen, H. (2000). Molecular Dynamics Simulations of Dodecylphosphocholine Micelles at Three Different Aggregate Sizes: Micellar Structure and Chain Relaxation. JOURNAL OF PHYSICAL CHEMISTRY A *104*, 6380-6388.
Tieleman, D.P., Forrest, L.R., Sansom, M.S., and Berendsen, H.J. (1998). Lipid properties and the orientation of aromatic residues in OmpF, influenza M2, and alamethicin systems: molecular dynamics simulations. Biochemistry *37*, 17554-17561.
van Gunsteren, W., and Berendsen, H. (1990). Computer Simulation of Molecular Dynamics: Methodology, Applications, and Perspectives in Chemistry. Angewandte Chemie International Edition in English *29*, 992-1023.
Xiang, Z., Soto, C.S., and Honig, B. (2002). Evaluating conformational free energies: the colony energy and its application to the problem of loop prediction. Proc Natl Acad Sci U S A *99*, 7432-7437.